Mesenchymal Stem Cell-Derived Exosomes Ameliorate Gentamicin-Induced Vestibular Hair Cell Injury by Regulating the SNARE Pathway and Enhancing Autophagy

Runnan Han[1#], Ning Yu[2#], GuoWei Qi[2], Jing Wang[1], Yanan Wu[1], Chuan Qin[1],Lin Shi[1*], Liang Wang[3*]

Affiliations:
[1] Department of Otorhinolaryngology, The First Hospital of Dalian Medical University, Dalian, Liaoning Province, China.
[2] Department of Otorhinolaryngology, The Sixth Medical Center of Chinese People's Liberation Army General Hospital, Beijing, China.
[3] Stem Cell Clinical Research Center, National Joint Engineering Laboratory, Regenerative Medicine Center, The First Affiliated Hospital of Dalian Medical University, Dalian, Liaoning Province, China.
*Corresponding authors:
Lin Shi
Address: Department of Otorhinolaryngology, The First Hospital of Dalian Medical University. No.222 Zhongshan Road, 116011, Dalian, China.
Email: shilin516@sina.com
Liang Wang
Address: Stem Cell Clinical Research Center, National Joint Engineering Laboratory, Regenerative Medicine Center, The First Affiliated Hospital of Dalian Medical University. 116012, Dalian, China. Email: wangliang@dmu.edu.cn
#Runnan Han and Ning Yu contributed equally to this work.

Mesenchymal Stem Cell-Derived Exosomes Ameliorate Gentamicin-Induced Vestibular Hair Cell Injury by Regulating the SNARE Pathway and Enhancing Autophagy

Abstract

Objective: To investigate the delivery efficiency of human umbilical cord mesenchymal stem cell-derived exosomes (hucMSC-EXOs) via intratympanic injection into vestibular end organs,evaluate their protective effects against gentamicin-induced vestibular dysfunction and hearing loss on gentamicin-induced vestibular dysfunction and hearing loss, and explore their regulatory mechanisms on hair cell apoptosis and autophagy.

Methods: Exosome characteristics were identified by transmission electron microscopy, nanoparticle tracking analysis, and Western blot. PKH26 labeling was used to trace their distribution in the vestibule. SD rats were randomly divided into four groups: control group, gentamicin group (GEN group), gentamicin+exosome group (GEN+EXO group), and gentamicin+dexamethasone group (GEN+DEX group). On day 6 after administration, vestibular function was assessed via open-field test and beam balance test. On day 7, high-frequency hearing (32 kHz) was detected by auditory brainstem response (ABR). The quantity and structural changes of hair cells were analyzed by immunofluorescence staining and scanning electron microscopy. Proteomics was used to analyze differentially expressed proteins in vestibular tissues treated with dexamethasone or hucMSC-EXOs. The regulatory effects on Caspase-3 (apoptosis) and LC3 (autophagy) were validated by immunofluorescence.

Results: hucMSC-EXOs administered via intratympanic injection were found to target the utricle, saccule, and crista ampullaris. Behavioral studies showed that the GEN+EXO group exhibited significant suppression of gentamicin-induced reduction in total movement distance ($p<0.05$) and movement speed ($p<0.05$, superior to the GEN+DEX group), with a 60.5% reduction in beam balance test passage time ($p<0.05$). ABR results revealed that the auditory threshold at 32 kHz in the GEN+EXO group was 18.3 dB SPL lower than that in the injury group ($p<0.01$), with no statistical difference compared to the GEN+DEX group. Hair cell counting showed significant protective effects of exosomes in reducing hair cell loss in the utricular striola (+25%), saccular striola (+44%), and central crista ampullaris (+44%), with partial regions outperforming the GEN+DEX group (e.g., 109% repair rate in the saccular striola). Scanning electron microscopy confirmed that exosomes reduced hair cell cilia loss and structural vacuolization. Proteomics showed

significant activation of the complement and coagulation cascades in the GEN group, while the GEN+EXO group enhanced autophagy via enriching the vesicle transport-related SNARE interaction pathway and improved energy metabolism and oxidative stress by regulating metabolic pathways. Immunofluorescence demonstrated that exosomes significantly reduced the expression of the apoptosis marker Caspase-3 ($p<0.01$) and enhanced the activity of the autophagy marker LC3 ($p<0.05$).

Conclusions: hucMSC-EXOs delivered via intratympanic injection effectively target vestibular sensory epithelia, significantly suppressing gentamicin-induced balance dysfunction and high-frequency hearing loss, with superior efficacy in partial indicators (e.g., movement speed, saccular hair cell repair) compared to dexamethasone.

hucMSC-EXOs exert protective effects through a dual mechanism of "anti-apoptosis and pro-autophagy," providing a novel therapeutic strategy for vestibular hair cell injury.

Keywords: Gentamicin ototoxicity; Vestibular dysfunction; Exosomes; intratympanic injection; Autophagy; Apoptosis.

1. Introduction

Gentamicin, an aminoglycoside antibiotic, is widely used in the treatment of severe bacterial infections [1]. However, its clinical use is often complicated by ototoxicity, particularly causing damage to vestibular and auditory hair cells in the inner ear [2, 3]. Studies have shown that gentamicin enters hair cells, leading to abnormal elevation of intracellular calcium concentrations and triggering oxidative stress responses [4]. Additionally, gentamicin induces mitochondrial dysfunction, increases the production of reactive oxygen species (ROS), and ultimately leads to cell death [5]. These complex biological mechanisms severely affect vestibular hair cells, causing symptoms such as vertigo and balance disorders in patients [6]. Currently, therapeutic options for gentamicin-induced vestibular hair cell injury remain relatively limited, with main strategies including early discontinuation of gentamicin and the use of protective agents such as antioxidants and neurotrophic factors [7]. Although some drugs have demonstrated protective effects on hair cells in research, no effective clinical treatment protocols have been established, making the development of novel interventions imperative.

In recent years, umbilical cord mesenchymal stem cells (UC-MSCs) have garnered extensive attention from researchers due to their excellent proliferation and differentiation capabilities, as well as superior immunomodulatory and tissue repair functions [8]. Beyond their own proliferation and differentiation potential, stem cells secrete extracellular vesicles containing various cytokines, which play critical roles in cell protection, regeneration, and repair of damaged tissues [9]. Existing studies have shown that UC-MSCs and their secreted exosomes can protect hair cells through multiple mechanisms, such as anti-apoptosis and promotion of autophagy [10]. Therefore, utilizing UC-MSC-derived exosomes to intervene in gentamicin-induced hair cell injury holds significant application potential and research value.

This study aims to establish an animal model of vestibular hair cell injury induced by gentamicin and subsequently administer exosome intervention. Through a combination of behavioral function assessments, immunofluorescence staining, scanning electron microscopy, proteomics, and other methods, quantitative and qualitative analyses of hair cell protection will be conducted. The goal is to observe the protective effects of exosomes on vestibular hair cells and elucidate the underlying molecular biological mechanisms.

2. Materials and Methods

2.1 Reagents and Antibodies

2.1.1 Reagents

Gentamicin (Sigma Aldrich, UK, G1272), 4% Paraformaldehyde (Biyuntian, China, P0099), 10% EDTA Solution (Sigma Aldrich, USA, E6758), PBS Buffer (Solarbio, China, P1020), Triton X-100 Solution (Sigma Aldrich, USA, T8787), 2.5% Glutaraldehyde (Coolaber, China, C0250), Electron Microscopy Fixative (Servicebio, USA, G1102), Isoamyl Acetate (Sinopharm Chemical Reagent Co., Ltd., China, 10009518), Anhydrous Ethanol (Sinopharm Chemical Reagent Co., Ltd., China, 10009218), Osmic Acid (Ted Pella Inc., USA, 18451), Sodium Pentobarbital (Beijing Pubos Biological Co., Ltd., China, PB001), Dexamethasone Sodium Phosphate Injection (Henan Runhong Pharmaceutical Co., Ltd., China, H41020015), DAPI (Zhongshan Jinqiao, China, ZLI-9557), PKH26 (Sigma, MINI26, MINI26-1KT), Phalloidin (Thermo Fisher Scientific, USA, A12380), Alexa Fluor 568 (Thermo Fisher Scientific, USA, A10042), Alexa Fluor 488 (Thermo Fisher Scientific, USA, A11008), Alexa Fluor 647 (Thermo Fisher Scientific, USA, A21245), Ammonium Bicarbonate (Sigma-Aldrich, St. Louis, MO, USA, 09830), Dithiothreitol (DTT) (Sigma-Aldrich, St. Louis, MO, USA, D9779), Iodoacetamide (IAA) (Sigma-Aldrich, St. Louis, MO, USA, I1149), Sodium Carbonate (Sigma-Aldrich, St. Louis, MO, USA, S7795), Urea (Bio-Rad, Hercules, CA, USA, 1610731), Sodium Dodecyl Sulfate (SDS) (Bio-Rad, Hercules, CA, USA, 1610302), Acetonitrile (J. T. Baker, Phillipsburg, NJ, USA, 9017-03), Water for nano-LC−MS/MS (J. T. Baker, Phillipsburg, NJ, USA, 9080-03), Trypsin (Promega, Madison, WI, USA, V5111), BCA Protein Concentration Assay Kit (Omiget, Omp-03, Omp-03-500T), Exosome Protein Extraction Kit (Omiget, Ome-04, Ome-04-50T).

2.1.2 Antibodies:

CD9 Antibody (Primary Antibody, CST, 13174, 13174S), TSG101 Antibody (Primary Antibody, CST, 72312, 72312S), CD63 Antibody (Primary Antibody, Bioswamp, PAB48050, PAB48050), Cleaved Caspase-3 Antibody (Primary Antibody, Cell Signaling Technology, USA, 9661S), LC3α/β Antibody (Primary Antibody, Shenyang Wanlei Biotechnology Co., Ltd., China, WL02013, WL02013), Anti-Rabbit Secondary Antibody (Secondary Antibody, Zhongshan Jinqiao, ZB-2301, ZB-2301).

2.2 Experimental Animals and Grouping

Twenty SPF-grade male Sprague-Dawley (SD) rats (250–300 g) were screened to exclude ear injuries and randomly divided into 4 groups (n=5 rats per group): control group, gentamicin injury group (GEN group), gentamicin+dexamethasone group (GEN+DEX group), and gentamicin+umbilical cord mesenchymal stem cell-derived exosome group (GEN+EXO group). Animals were provided by Beijing

Keyu Animal Breeding Co., Ltd. and housed in the Animal Center of the Chinese People's Liberation Army General Hospital under controlled conditions: (23±2)°C, (55±10)% humidity, 12-h light/dark cycle, with free access to food and water. The experiment was approved by the Animal Care and Use Committee of the Chinese People's Liberation Army General Hospital (Ethics Approval No.: S2020-465-01), and the detailed workflow is shown in Figure 1.

2.3 solation of hUC-MSCs-Derived Exosomes

Human Umbilical Cord Mesenchymal Stem Cells (hUC-MSCs) were seeded in α-MEM or DMEM/F12 medium containing pre-treated exosome-depleted fetal bovine serum (FBS), and cultured at 37°C in a 5% CO_2 incubator until the cell confluency reached over 65%. After that, the original medium was discarded, and the cells were washed once with PBS. Fresh exosome-free medium was then added to continue culturing for 24–72 hours (to ensure the final cell confluency reaches approximately 90% with significant proliferation, and the maximum culture duration does not exceed 72 hours). Subsequently, cell supernatants were collected and subjected to sequential centrifugation steps: centrifuged at 300×g and 4°C for 10 minutes (to discard intact cells), then at 3000×g and 4°C for 10 minutes (to discard cell debris), and further at 10,000×g and 4°C for 10 minutes (to discard large vesicle impurities) to obtain the crude exosome extract. Immediately after, the crude extract was filtered through a 0.22 μm filter membrane to remove residual tiny impurities.

The filtrate was mixed with pre-treated hydroxyl-modified magnetic beads (0.6 ml of magnetic beads were centrifuged at 3000×g and 4°C for 2 minutes first, then resuspended with pre-chilled PBS), and incubated with rotation at 4°C for 60 minutes. After incubation, the magnetic beads were precipitated by centrifugation at 3000×g and 4°C for 5 minutes. The supernatant was discarded, and the magnetic beads were washed twice with pre-chilled PBS. Next, 0.8–1.5 ml of elution buffer (Buffer EXE) was added, followed by vigorous vortexing for 30 seconds. The mixture was then centrifuged at 7000×g and 4°C for 2 minutes, and the supernatant was collected and further centrifuged at 12,000×g and 4°C for 2 minutes for additional purification, yielding the exosome solution finally.

2.4 Intratympanic injection

Rats were anesthetized via intraperitoneal injection of pentobarbital (50–60 mg/kg). Under a surgical microscope (Olympus5A, Japan), drugs were injected into the anteroinferior quadrant of the tympanic membrane. The control group received 50 μL of normal saline; the GEN group received 50 μL of 40 mg/mL gentamicin; the GEN+DEX group received a 50 μL mixture of gentamicin and dexamethasone (25 μL gentamicin [80 mg/mL] + 25

μL dexamethasone [5 mg/mL]); the GEN+EXO group received a 50 μL mixture of gentamicin and exosomes (25 μL gentamicin [80 mg/mL] + 25 μL exosome solution [4.4×10^{10} particles/mL]).

2.5 Behavioral Tests for Balance Function

Vestibular balance ability was assessed via the beam balance test and open-field test. The open-field test was conducted in a 75 cm×75 cm soundproof arena. Rat movements were recorded for 7 minutes, and trajectories were analyzed using DeepLabCut software (marking key points: head, trunk, tail root) to extract parameters such as path length and speed.

The beam balance test used an 110 cm-long, 1 cm-wide elevated beam with foam boxes at both ends. The test began when the rat's forepaws touched the starting line and ended when the forepaws reached a mark 10 cm from the box (to avoid errors from sniffing). Test parameters included passage time, falls, and abnormal behaviors. Equipment was disinfected, and bedding was replaced after each test.

2.6 Auditory Brainstem Response (ABR) Testing

In a soundproof chamber, rats were anesthetized with 1% pentobarbital sodium (0.1 g□kg^{-1} via intraperitoneal injection) and placed on a 37°C temperature-controlled blanket. Recording, ground, and reference electrodes were inserted subcutaneously at the vertex, below the sound-presenting ear, and below the contralateral ear, respectively. Short pure-tone stimuli at 8 kHz, 16 kHz, 24 kHz, and 32 kHz were delivered using a Tucker-Davis Technology-Ⅲ (TDT-Ⅲ) system with a filter bandwidth of 300–3,000 Hz and 500 sweeps. Stimulation intensity started at 90 dB sound pressure level (SPL) and decreased by 5 dB increments. The ABR hearing threshold was defined as the highest intensity at which the Wave Ⅱ waveform was still detectable.

2.7 Tissue Sampling of Vestibular End Organs

After completion of the final ABR test, all experimental animals were euthanized via decapitation as follows:

Prior to euthanasia, rats were deeply anesthetized with 1% sodium pentobarbital (0.1 g·kg^{-1} body weight, intraperitoneal injection). Once the absence of paw pinch withdrawal reflex and corneal reflex was confirmed, decapitation was performed using a sterile, sharp guillotine designed for small laboratory animals to ensure rapid and painless termination, in compliance with the ethical guidelines approved by the Animal Care and Use Committee of the PLA General Hospital (Approval No. S2020-465-01).

Soft tissues were removed, and the cochlea was exposed. The cochlear apex and oval window were punctured to perfuse paraformaldehyde (for immunofluorescence) or glutaraldehyde (for

scanning electron microscopy [SEM]) through the apex for fixation. Samples were stored at 4°C overnight. The next day, the utricular macula, saccular macula, and crista ampullaris were dissected, and otolithic membranes were removed for subsequent immunofluorescence staining and SEM observation.

2.8 Exosome Identification and Tracing

Human umbilical cord mesenchymal stem cell-derived exosomes (hucMSC-EXOs) were identified by transmission electron microscopy (TEM, Hitachi, Japan), nanoparticle tracking analysis (NTA, Particle Metrix ZETAVIEW, Germany), and Western blot. Exosomes were labeled with PKH26, co-injected with gentamicin into the tympanic cavity of anesthetized rats, and traced after 7 days. Tissues were fixed via perfusion with paraformaldehyde, and the utricular macula, saccular macula, and crista ampullaris were dissected for immunofluorescence staining and observation under a laser confocal microscope (Olympus FV1000, Japan).

2.9 SEM Sample Preparation and Morphological Observation

After decapitation, auditory bullae were rapidly dissected and fixed with glutaraldehyde. The next day, the utricular macula, saccular macula, and crista ampullaris were dissected, and otolithic membranes were removed. Samples were rinsed 3 times with 0.1M phosphate buffer (PB, pH 7.4) for 15 min each, fixed with 1% osmium tetroxide in the dark for 2 h, and rinsed again. Samples were further fixed with 2% tannic acid for 1 h, re-fixed with 1% osmium tetroxide for 1 h (dark), rinsed with PB, dehydrated in a graded ethanol series (50%, 70%, 90%, 100%; two times per concentration, 15 min each), and treated with isoamyl acetate for 15 min. After critical point drying, samples were mounted on conductive carbon tape, sputter-coated with gold for 30 s (HITACHI MC1000), and observed under SEM (HITACHI SU8100, Japan).

2.10 Immunofluorescence Staining for Vestibular Hair Cell Cilia

Vestibular end organ specimens were rinsed with 0.1M PBS, blocked with 10% goat serum for 1 h, rinsed with PBST, and stained with 100 μL Phalloidin solution in the dark for 1 h. After rinsing with PBST and PBS, samples were mounted with DAPI for nuclear staining.

2.11 DIA Proteomics Mass Spectrometry Analysis

Utricular maculae were lysed with SDT lysis buffer (4% SDS, 100 mM DTT), boiled, sonicated, and centrifuged at 16,000g to collect supernatants. Protein concentration was determined by BCA assay. Plasma samples were denatured with urea, reduced with DTT, alkylated with IAA, and digested with trypsin (enzyme-substrate ratio 50:1) overnight. Peptides were desalted with C18 columns and analyzed by Orbitrap Astral mass spectrometry (coupled with

Vanquish UHPLC) in data-independent acquisition (DIA) mode using an 8-min gradient of 0.1% formic acid-acetonitrile. Data were searched against the UniProtKB database using DIA-NN with parameters including trypsin digestion, 10 ppm mass tolerance, and FDR<1%. Clustering, volcano plot analysis, GO/KEGG enrichment ($p<0.01$), and PPI network construction (STRING/Cytoscape) were performed using R language.

2.12 Immunofluorescence Staining for Caspase-3 and LC3

Vestibular end organs were permeabilized with 0.1% Triton for 30 min, washed 3 times with PBS (5 min each), blocked with goat serum for 1 h, and incubated with primary antibodies against cleaved Caspase-3 (apoptosis marker) and LC3α/β (autophagy marker) at 4°C overnight. After washing with PBST (3×10 min), samples were incubated with Alexa Fluor 647-conjugated secondary antibodies for 1 h, washed, and mounted with DAPI.

2.13 Image Acquisition and Processing

Images were acquired using an Olympus FV1000D laser scanning confocal microscope. Low-magnification (5× or 10×) images were first used to locate the sample area, followed by 10× overview images and 100× high-magnification images of selected fields. Z-stack scanning was performed to capture cells across different focal planes. Images were processed with FV31S-SW software for scale bar addition and Image J for layer overlay and channel integration.

2.14 Vestibular Hair Cell Counting

Images were organized and analyzed using ImageJ software. Samples were derived from the vestibular end organs of 5 SD rats per group as designed in the experiment. For each rat, 6 counting grids of 50 μm^2 were selected from the striolar region (S), medial extrastriola (MES), and lateral extrastriola (LES) of the utricular macula, respectively; 6 counting grids of 50 μm^2 were selected from the striolar region (S) and extrastriola (ES) of the saccular macula, respectively; and 3 counting grids of 50 μm^2 were selected from the crista ampullaris. All counting grids were chosen by a trained blinded observer (Observer A) via random sampling. Another trained blinded observer (Observer B) performed image quality control using the double-blind method, strictly excluding invalid images with visual field defects, impurity interference, or obscure cell boundaries that were difficult to distinguish. Using the minimum number of effective images per region per group as the unified standard, the final effective sample sizes were determined as follows: 24 images per region for each area of the utricular macula, 18 images per region for each area of the saccular macula, and 9 images for the central region of the crista ampullaris. Counting was conducted in accordance with the grid boundary principle of "counting cells touching the top and

left boundaries but not the bottom and right ones." Prior power analysis results indicated that the sample size of 5 SD rats per group provided sufficient statistical power (power=0.8), which could effectively detect statistical differences among groups and meet the statistical test requirements of the experimental design.

2.15 Quantitative Analysis of Caspase-3 and LC3 Immunofluorescence

Fluorescence images were converted to 8-bit grayscale in Image J. Regions of interest (ROI) were selected with a rectangular tool, background-subtracted (rolling ball radius 50 pixels), and thresholded using Otsu's algorithm. For groups with high fluorescence variability, the threshold was set to background mean + 2×SD. Integral density was measured, divided by ROI area to obtain mean fluorescence intensity, normalized, and imported into Excel.

2.16 Statistical Analysis

Data were analyzed and plotted using GraphPad Prism 9.5.1. One-way ANOVA was used for open-field test, beam balance test, and fluorescence intensity data; two-way ANOVA was used for hearing thresholds and hair cell counts. Data were first tested for normality (Shapiro-Wilk test) and homogeneity of variance. For normally distributed data with homogeneous variance, ANOVA was followed by Tukey's post hoc test. For non-normal or heteroscedastic data, Kruskal-Wallis test was used, followed by Dunn's post hoc test. Statistical significance was defined as *p<0.05, **p<0.01, ***p<0.001, ****p<0.0001.

2.17 Statement

The design, implementation, and reporting of this study strictly adhere to the core requirements of the ARRIVE Guidelines 2.0 (Animal Research: Reporting of In Vivo Experiments).

Figure 1 Experimental Flowchart

3. Results

3.1 Exosome Identification and Tracing Experiments

3.1.1 Exosome Identification Results

The isolated hucMSC-EXOs were characterized as follows. Under transmission electron microscopy (TEM), round or cup-shaped membranous vesicles with clear boundaries were clearly observed, exhibiting morphological features consistent with typical exosomes (Figure 2A). Nanoparticle tracking analysis (NTA) revealed that the average particle size of the vesicles was 122.0 nm, falling within the characteristic size range of exosomes (30–150 nm) (Figure 2B). Western blot analysis confirmed the expression of exosome-specific marker proteins CD9, TSG101, and CD63 (Figure 2C).

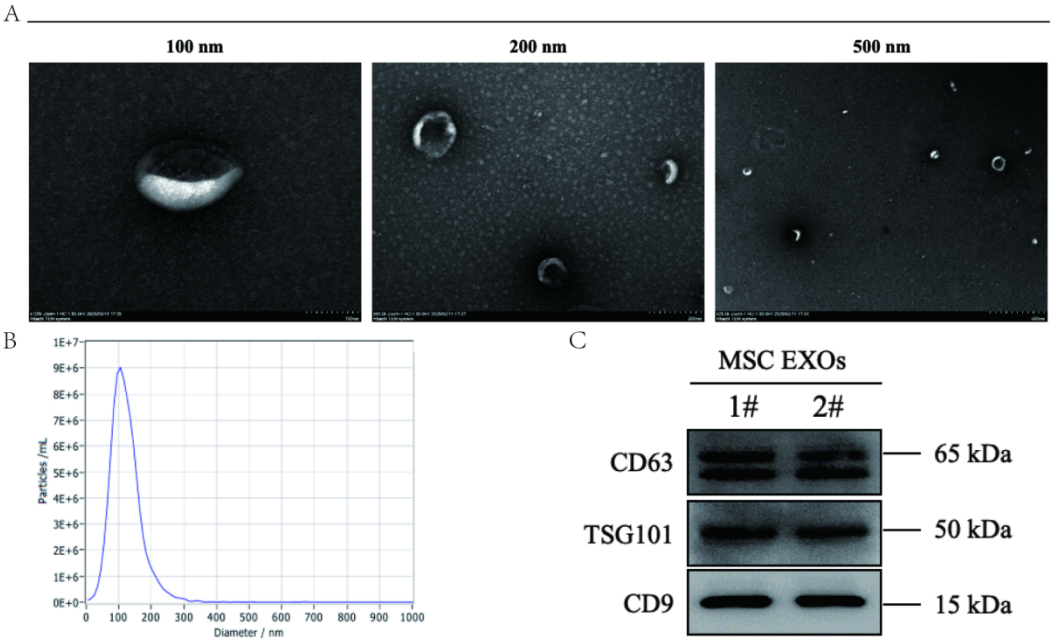

Figure 2 Identification of exosomes

A: Transmission electron microscopy (TEM) imaging. Images were captured at 100 nm, 200 nm, and 500 nm scales to observe the morphology of hucMSC-EXOs. B: Nanoparticle tracking analysis (NTA) for determining the particle size distribution of hucMSC-EXOs. The average particle size of EXOs was 122.0 nm, with a main peak at 107.7 nm (accounting for 99.2% of the total particles), and the final concentration was 4.4×10^{10} particles/mL.C: Western blot analysis to detect the expression of exosomal marker proteins CD9, TSG101, and CD63.

3.1.2 Exosomes Delivered via intratympanic injection Reach the Sensory Epithelium of the Utricle, Saccule, and Crista Ampullaris

PKH26-stained hucMSC-EXOs were clearly detectable in the utricular macula, saccular macula, and crista ampullaris (Figure 3).

Under fluorescence microscopy, they appeared as scattered, small-diameter round or oval fluorescent spots, characteristic of immunofluorescence-stained exosomes. In addition to these exosome-specific fluorescence signals, red fluorescence was observed in the cytoskeleton of some cellular regions. This phenomenon may suggest that exosomes had been internalized by cells. Upon cellular uptake, the PKH26 dye likely entered cells with exosomes and diffused intracellularly, leading to staining of partial cytoskeletal regions.

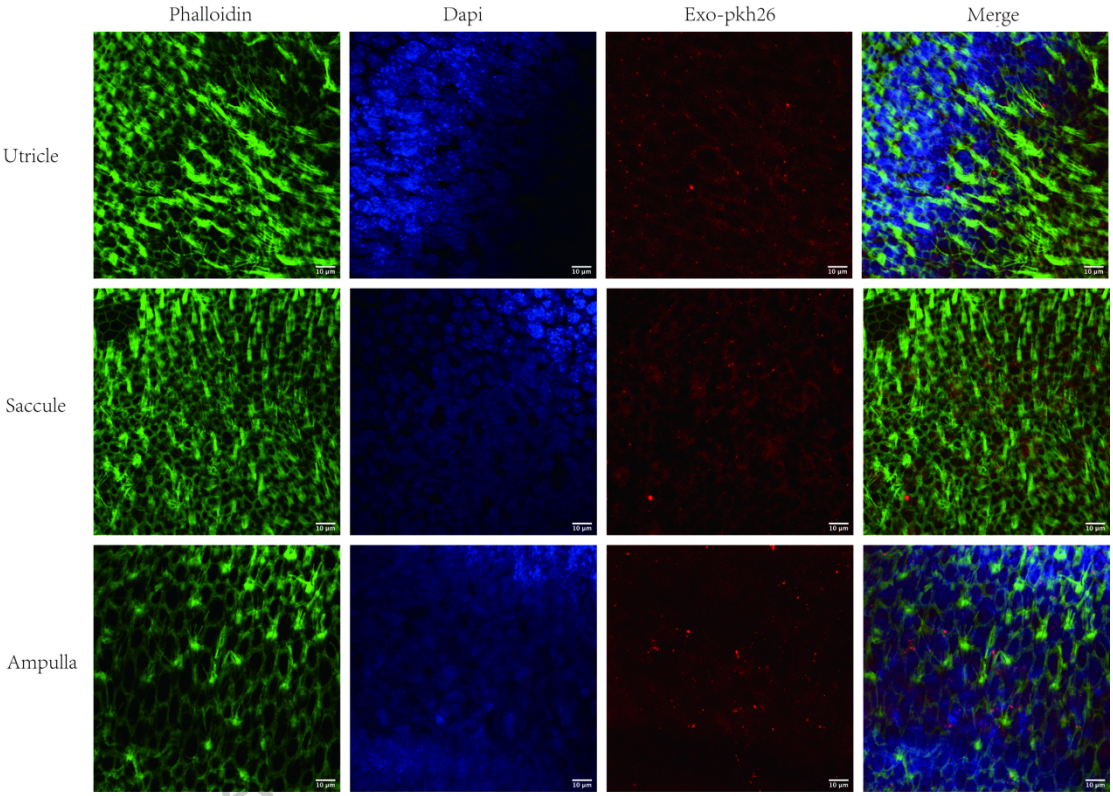

Figure 3 Distribution of exosomes in the utricular macula, saccular macula, and crista ampullaris.

Green fluorescence: Phalloidin staining marking hair cell stereocilia;Red fluorescence: PKH26 staining marking exosomes;Blue fluorescence: DAPI staining marking cell nuclei.

3.2 Behavioral Experiments Demonstrate Exosomes Improve Vestibular Dysfunction Caused by Gentamicin-Induced Vestibular Hair Cell Injury

3.2.1 Exosomes Enhance Locomotor Activity in Open-Field Test After Gentamicin Injury

Autonomous activity and exploratory behavior were assessed via the open-field test. Heat maps (Figure 4A-D) and track plots (Figure 4E-H) visually represented activity patterns across groups. Control rats exhibited extensive activity with richly colored heat maps and complex, wide-ranging tracks, indicating high autonomous activity and exploratory motivation. In the GEN group, heat maps were dim

and concentrated in corners, with monotonous and restricted tracks, demonstrating significant inhibition of autonomous activity and exploration by gentamicin. The GEN+EXO and GEN+DEX groups showed intermediate performance comparable to each other.

For total movement distance (Figure 4I), the control group had the highest value, the GEN group the lowest, with GEN+EXO and GEN+DEX intermediate. The GEN+EXO group showed a significant increase compared to the GEN group ($p<0.05$), indicating exosome treatment effectively improved autonomous activity.

In movement speed (Figure 4J), the control group had the fastest speed, the GEN group the slowest, with GEN+EXO and GEN+DEX intermediate. The GEN+EXO group showed a significant increase compared to the GEN group ($p<0.05$), while no significant difference was observed between GEN+DEX and GEN groups, suggesting exosomes specifically enhanced locomotor speed.

For the number of center zone entries (Figure 4K), the control group had the highest frequency. No significant differences were found between GEN+EXO/GEN+DEX and GEN groups, but both treatment groups showed significant reduction compared to the control group ($p<0.01$), indicating neither treatment restored exploratory behavior (measured by center zone entries) to normal levels.

In summary, the control group showed normal activity, while the GEN group exhibited significantly reduced total movement distance, speed, and center zone entries. The GEN+EXO and GEN+DEX groups did not differ in total distance or center entries, but GEN+EXO uniquely improved movement speed compared to GEN, whereas GEN+DEX had no effect. Neither treatment significantly restored exploratory behavior.

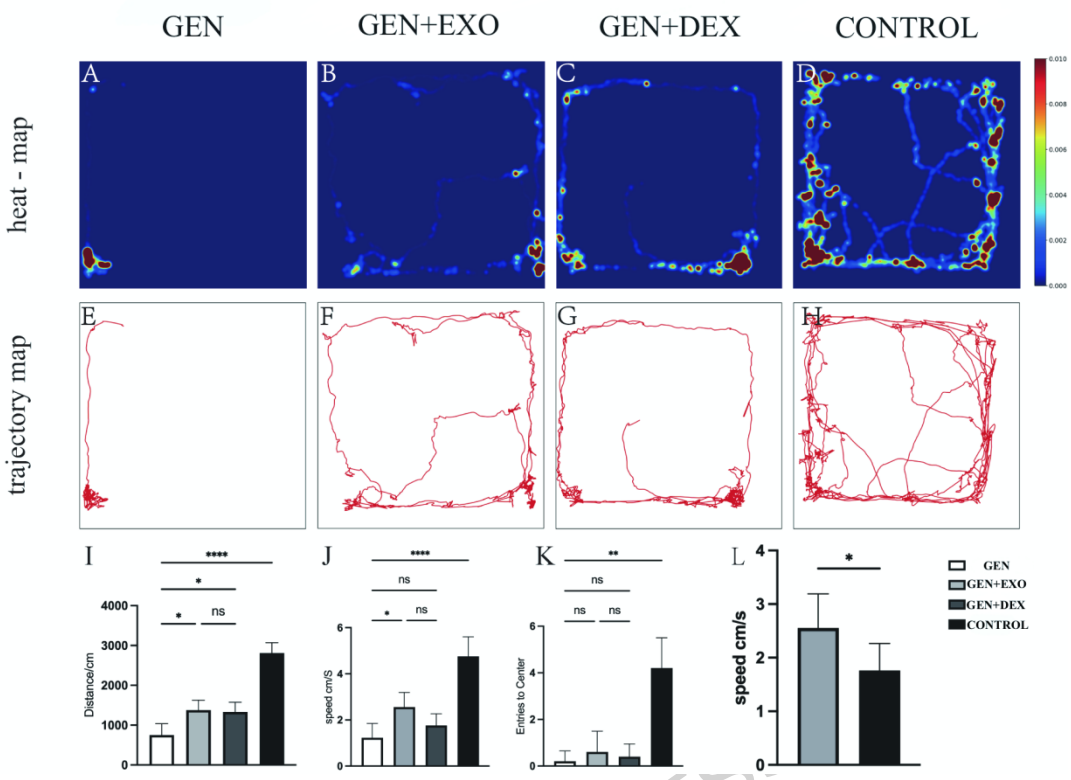

Figure 4 Open-field test.

A-D: Heat maps corresponding to the GEN group, GEN+EXO group, GEN+DEX group, and control group, respectively;E-H: Movement trajectory plots of the above groups;I: Comparison of total movement distance among groups;J: Comparison of movement speed among groups;K: Comparison of the number of center zone entries among groups;L: Statistical plot of the one-tailed t-test for movement speed between the GEN+EXO and GEN+DEX groups in the open-field test.*p < 0.05, **p < 0.01, ****p < 0.0001; ns: no significant difference.

3.2.2 Exosomes Reduce Beam Balance Test Passage Time in Gentamicin-Injured Rats

During the beam balance test, rats exhibited three typical movement patterns (Figure 5A-C): smooth passage (Figure 5A, stable limb contact and fluid movement), hindlimb dragging (Figure 5B, partial hindlimb detachment with slowed speed), and falling/struggling (Figure 5C, repeated hindlimb falls and labored progression). Balance and coordination were quantified as follows. On day 6 (Figure 5D), the GEN group took an average of 23.83 seconds to traverse the beam, significantly longer than the control group (8.400 seconds, $p<0.01$), confirming gentamicin-induced balance dysfunction. The GEN+EXO group required 9.400 seconds ($p<0.01$ vs. GEN), and the GEN+DEX group 12.00 seconds ($p<0.05$ vs. GEN), both significantly shorter than GEN, indicating both treatments improved balance. No significant difference was observed between GEN+EXO and GEN+DEX.

By day 6, while control rats shortened passage time due to practice, the GEN group showed persistent prolongation, confirming sustained balance impairment. Comparative analysis of day 3 and day 6 data demonstrated gentamicin-induced balance dysfunction, with both exosome and dexamethasone treatments effectively improving performance. Exosomes showed notable advantages in restoring balance function impaired by gentamicin.

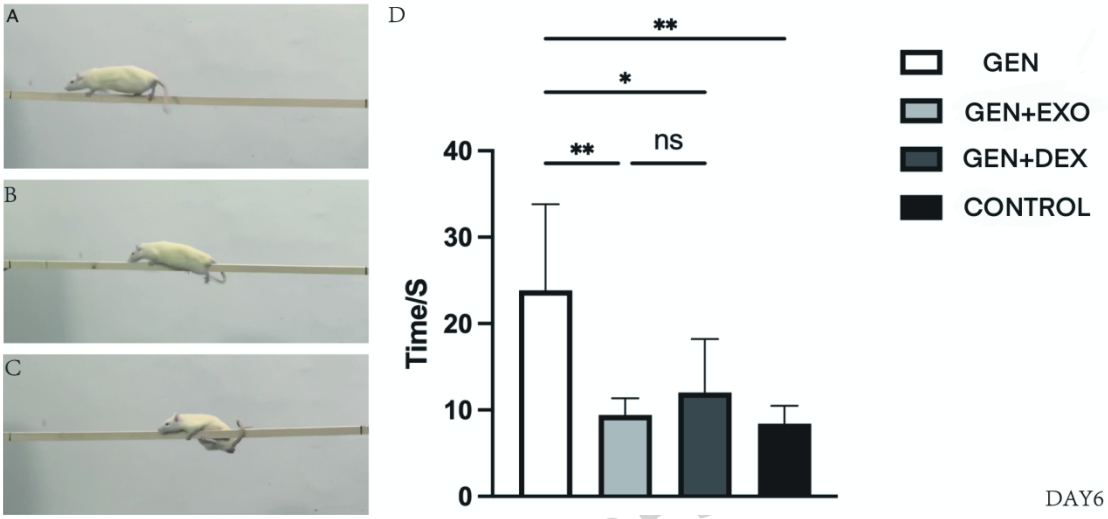

Figure 5 Beam balance test.

A-C: Postures of rats with different vestibular function on the beam; D: Bar chart of beam transit time on Day 6.

3.3 Exosomes Alleviate Gentamicin-Induced Hearing Loss

Auditory brainstem response (ABR) thresholds at various frequencies were measured on Day 7 (D7) to assess hearing changes. No significant differences in ABR thresholds were observed among the four groups under click sound and 4 kHz, 8 kHz, 16 kHz, or 24 kHz frequency stimuli. At 32 kHz, the ABR threshold was 55.00±6.32 dB SPL in the GEN group, 36.67±5.16 dB SPL in the GEN+EXO group, 39.167±10.20 dB SPL in the GEN+DEX group, and 22.50±5.24 dB SPL in the control group (Figure 6). Both the GEN+EXO and GEN+DEX groups exhibited significantly lower thresholds than the GEN group ($p<0.01$), but no significant difference was found between the GEN+EXO and GEN+DEX groups. These results indicate that both exosomes and dexamethasone improve gentamicin-induced high-frequency (32 kHz) hearing impairment. Although exosomes showed a slightly superior protective effect on hearing compared to dexamethasone, this difference did not reach statistical significance.

Group	Click	4kHz	8kHz	16kHz	24kHz	32kHz
GEN	42.50±9.3	44.17±5.85	33.33±7.5	31.67±8.1	37.50±6.8	55.00±6.32

	5		3	7	9	
GEN+EXO	40.83±8.01	44.17±9.70	35.83±7.36	30.00±4.47	34.17±3.76	36.67±5.16
GEN+DEX	46.67±8.76	48.33±9.31	35.83±8.01	30.83±4.92	34.17±8.61	39.167±10.20
CONTROL	29.17±5.85	38.33±14.02	26.67±5.16	17.50±5.24	20.00±3.16	22.50±5.24
p	0.980	>019999	0.9392	0.9807	0.8690	0.0003***

Data are presented as mean ± standard deviation (Mean ± SD). ***p < 0.001 indicates comparison between the GEN+EXO group and the GEN group.

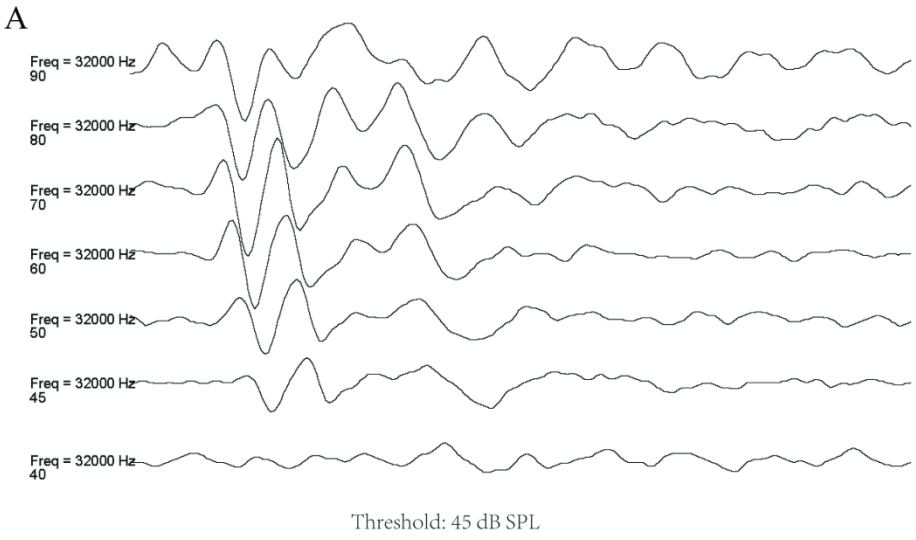

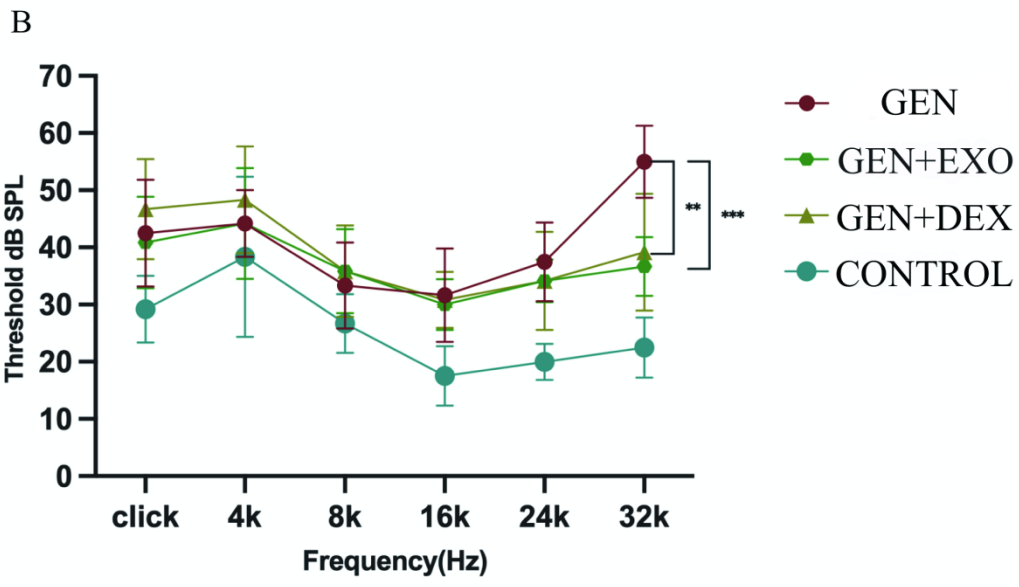

Figure 6. Auditory brainstem response (ABR) results

A:Representative ABR waveforms. B:Auditory brainstem response (ABR) thresholds of rats in different groups on day 7.The x-axis represents acoustic stimulus frequency (Hz), including click, 4 kHz, 8 kHz, 16 kHz, 24 kHz, and 32 kHz; the y-axis represents ABR threshold (dB SPL). ** indicates $p < 0.01$ vs. GEN group; *** indicates $p < 0.001$ vs. GEN group.

3.4 Exosomes can alleviate gentamicin-induced reduction of vestibular hair cells

Analysis of hair cell staining images showed that in the control group, hair cells in the utricular macula were densely arranged with higher counts across regions: the striolar region (S) had a mean of 13.292±2.645, the medial extrastriola (MES) 9.000±1.532, and the lateral extrastriola (LES) 22.833±3.975. In the GEN group, hair cell counts in the S and MES regions were significantly lower than those in the control group ($p < 0.0001$), with means of 7.833±1.465 (S) and 5.292±1.301 (MES) , while the LES region showed no significant difference from the control group ($p > 0.05$, mean=22.125±3.567,). The GEN+EXO group exhibited significantly higher hair cell counts in the S region compared to the GEN group ($p < 0.05$, mean=9.792±2.340,), but no significant difference was observed in the MES region ($p > 0.05$, mean=6.833±1.523,); the LES region showed no significant difference from the control group ($p > 0.05$, mean=22.042±2.956,). The GEN+DEX group had significantly higher hair cell counts in both the S and MES regions than the GEN group (means=11.083±2.320 for S and 8.208±1.615 for MES,), with no significant difference in the LES region (mean=21.958±2.926,) (Figure 7E).

For the saccular macula, the control group showed normal hair cell morphology and higher counts, with means of 10.000±1.495 in the striolar region (S) and 16.278±1.904 in the extrastriola (ES) . The GEN group exhibited significantly lower hair cell counts in both regions compared to the control group ($p < 0.001$), with means of 5.444±1.338 (S) and 10.944±3.733 (ES) . Both the GEN+EXO and GEN+DEX groups showed higher hair cell counts in these regions than the GEN group but lower than the control group ($p < 0.05$): the GEN+EXO group had means of 7.833±1.855 (S) and 12.444±2.895 (ES) , while the GEN+DEX group had means of 7.167±1.855 (S) and 11.556±2.307 (ES) (Figure 7F).

In the crista ampullaris, the control group had relatively high hair cell counts (mean=7.778±1.093,). The GEN group showed significantly lower hair cell counts than the control group ($p < 0.001$, mean=4.556±1.590,). Both the GEN+EXO and GEN+DEX groups exhibited higher hair cell counts than the GEN group ($p < 0.05$), with means of 6.556±1.509 (GEN+EXO,) and 7.333±1.414 (GEN+DEX,);

the GEN+DEX group was closer to the control group level (Figure 7G).

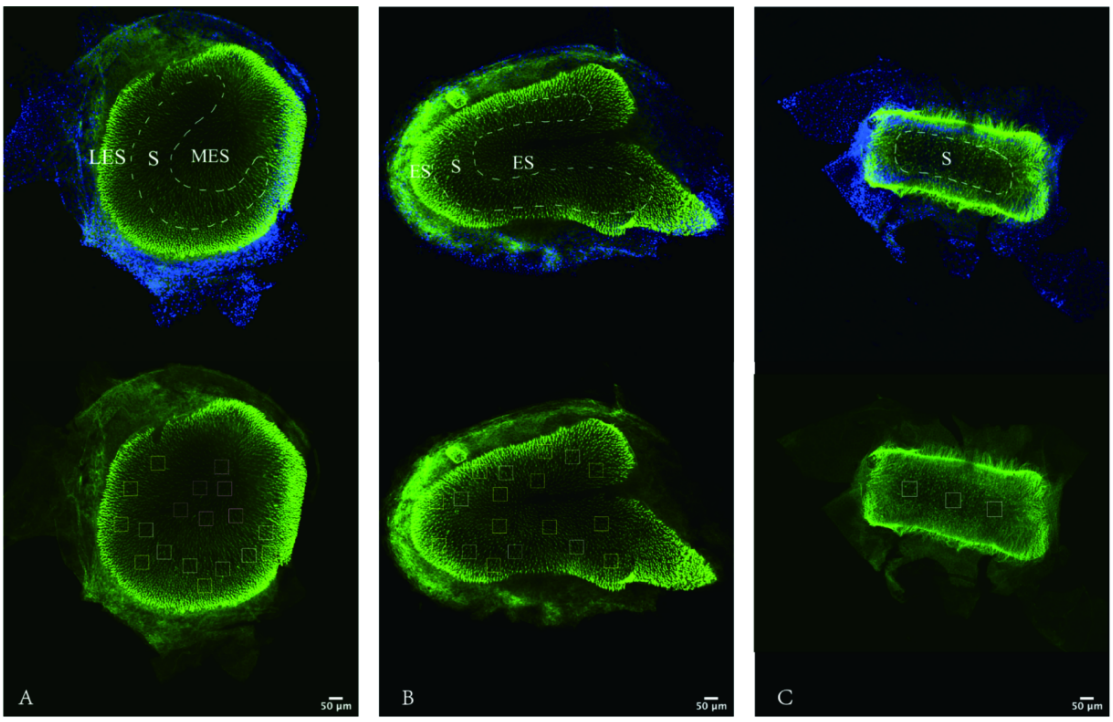
LES
S
MES
A
50 µm
ES
S
ES
B
50 µm
S
C
50 µm

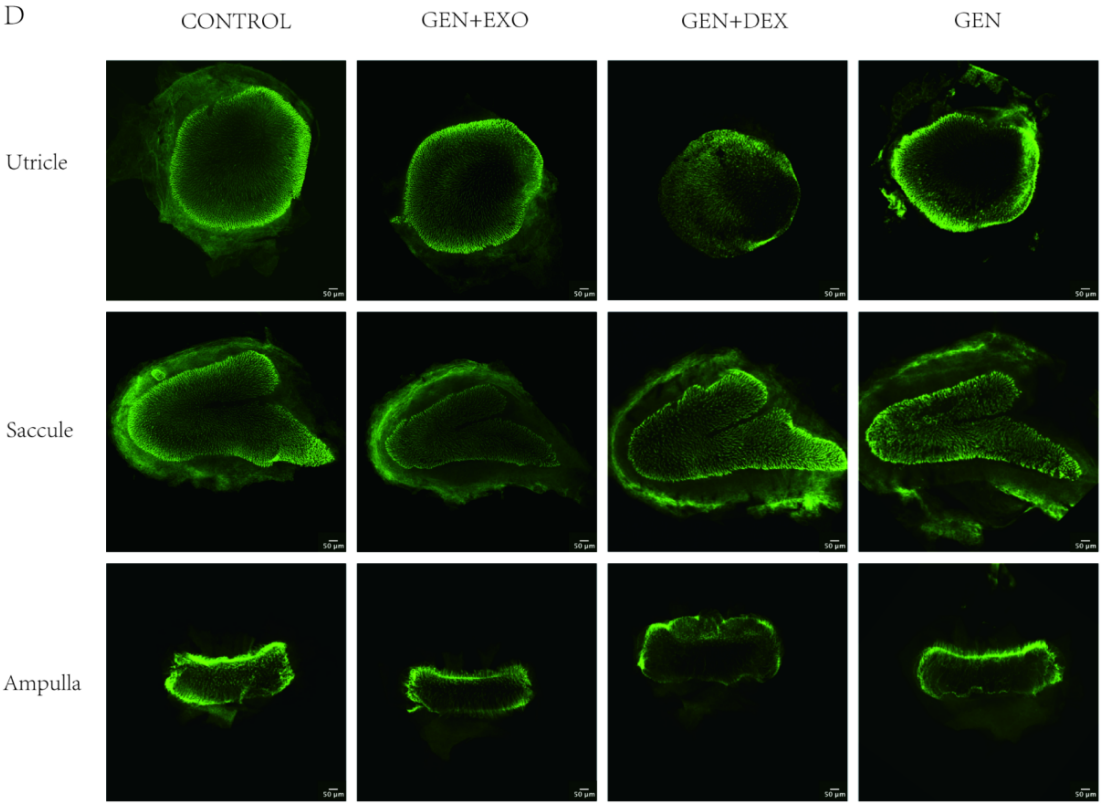
D
CONTROL
GEN+EXO
GEN+DEX
GEN
Utricle
Saccule
Ampulla

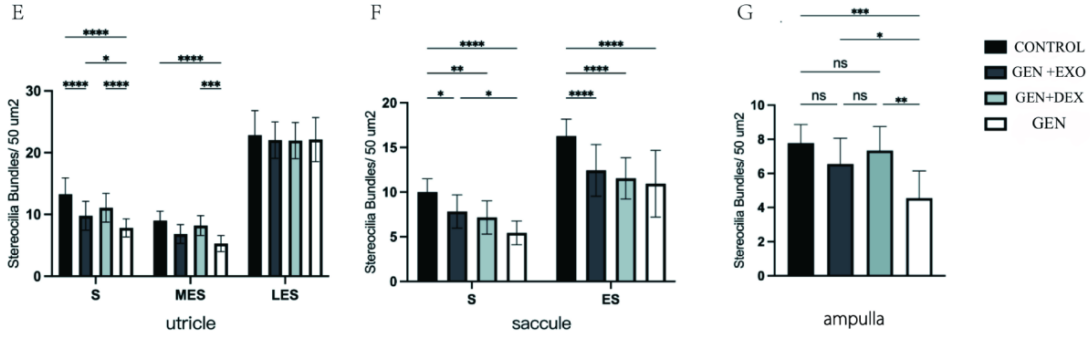
E
Stereocilia Bundles/ 50 um2
S
MES
LES
utricle
F
Stereocilia Bundles/ 50 um2
S
ES
saccule
G
Stereocilia Bundles/ 50 um2
ampulla
CONTROL
GEN +EXO
GEN+DEX
GEN

Figure 7 Vestibular hair cell counting.

A-C: Schematic diagrams of regional partitioning in the utricular macula, saccular macula, and crista ampullaris. White dashed lines mark the boundaries of subregions; S: striolar region; MES: medial extrastriolar region of the utricle; LES: lateral extrastriolar region of the utricle; ES: extrastriolar region of the saccule. Scale bar: 50 μm.D: Phalloidin immunofluorescence images of vestibular tissue stereocilia in different treatment groups.E-G: Statistical bar charts of hair cell counts in different regions of the utricular macula, saccular macula, and crista ampullaris, respectively. Data are presented as mean ± standard deviation (Mean ± SD); N: number of samples. *p < 0.05, **p < 0.01, ***p < 0.001, ****p < 0.0001; ns: no significant difference.

3.5 Exosomes Reduce Cilia Loss and Structural Vacuolization in Vestibular Hair Cells Caused by Gentamicin

Under scanning electron microscopy (SEM), the control group (Figure 8A) showed densely and regularly arranged hair cells on the surface of vestibular tissues, with intact cilia structures and normal microscopic morphology. In the GEN group (Figure 8B), compared with the control group, the number of hair cells was significantly reduced, and numerous pitted cavities appeared on the tissue surface, presumably as residual traces of hair cell cilia loss, indicating severe structural damage to hair cells by gentamicin. Compared with the GEN group, the GEN+DEX group showed improved reduction in hair cells, with fewer pitted cavities on the tissue surface (Figure 8C), suggesting that dexamethasone alleviated gentamicin-induced hair cell damage to some extent and facilitated structural repair of hair cells. The GEN+EXO group also exhibited improvement in gentamicin-induced damage, with relatively neat tissue surface structures and fewer pitted cavities compared to the GEN group, demonstrating the repair effect of exosomes on damaged hair cell structures (Figure 8D).

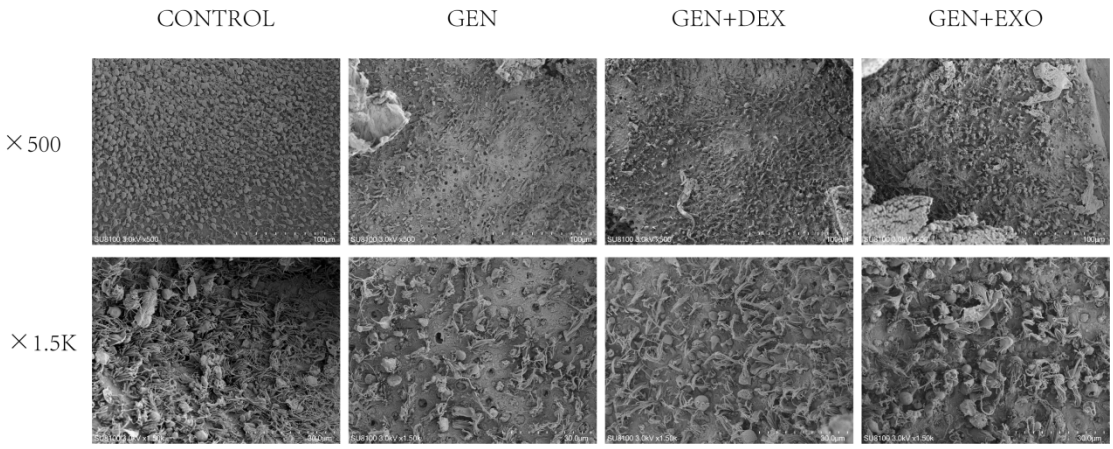

Figure 8 Scanning electron microscopy (SEM) images of utricular hair cells.

3.6 Proteomics Analysis Results

Principal component analysis (PCA, Figure 9A) showed significant

separation of protein expression profiles between the gentamicin injury group (GENT) and the control group, with tight clustering of normal group samples, indicating good model reproducibility and global changes in vestibular tissue protein expression induced by gentamicin. Samples in the GEN+EXO group migrated toward the normal group, narrowing the distance from the injury group, while the GEN+DEX group showed a similar trend, with the GEN+EXO group more closely approximating the normal group distribution.

Differentially expressed protein enrichment analysis (Figure 9B) identified metabolic pathways as the most significantly enriched category, involving dysregulation of proteins related to energy metabolism, oxidative stress, and mitochondrial function. Endocytosis was also significantly enriched.

KEGG pathway analysis revealed that compared with the control group, the GEN group showed the most significant difference in the complement and coagulation cascades pathway (Figure 9C). Compared with the GEN group, the GEN+EXO group was significantly enriched in SNARE interactions in vesicular transport and vasopressin-regulated water reabsorption pathways (Figure 9D). When comparing the GEN+EXO group with the GEN+DEX group, the proteasome pathway was the main differentially enriched pathway (Figure 9E).

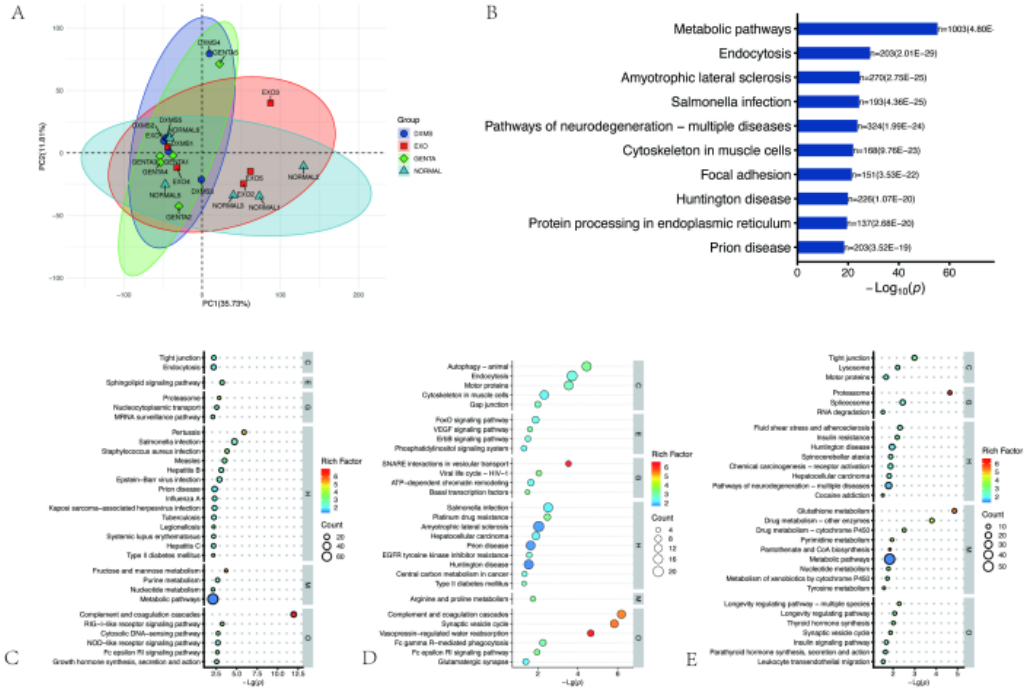

Figure 9 Proteomics analysis results

A: Protein expression profiles between the GEN group and control group; B: Enrichment analysis of differentially expressed proteins between the GEN group and control group; C: KEGG enrichment analysis of differentially expressed proteins between the GEN group and control group; D: Enrichment analysis of differentially expressed proteins between the

GEN+EXO group and GEN group; E: Enrichment analysis of differentially expressed proteins between the GEN+EXO group and GEN+DEX group.

3.7 Exosomes Alleviate Apoptosis and Enhance Autophagy in Gentamicin-Injured Vestibular Hair Cells

As shown in Figures 10A-B, the control group exhibited low Caspase-3 fluorescence intensity, indicating basal apoptosis at physiological levels. Following gentamicin intervention, Caspase-3 fluorescence signals significantly increased, with mean fluorescence intensity showing a highly significant difference compared to the control group ($p<0.0001$), demonstrating that gentamicin effectively induces vestibular hair cell apoptosis. Notably, both the exosome-treated and dexamethasone-treated groups showed significantly reduced Caspase-3 fluorescence intensity compared to the GEN group ($p<0.005$). Although the mean fluorescence intensity in the GEN+EXO group remained significantly higher than that in the control group ($p<0.001$), no statistical difference was observed between the GEN+EXO and GEN+DEX groups ($p>0.05$).

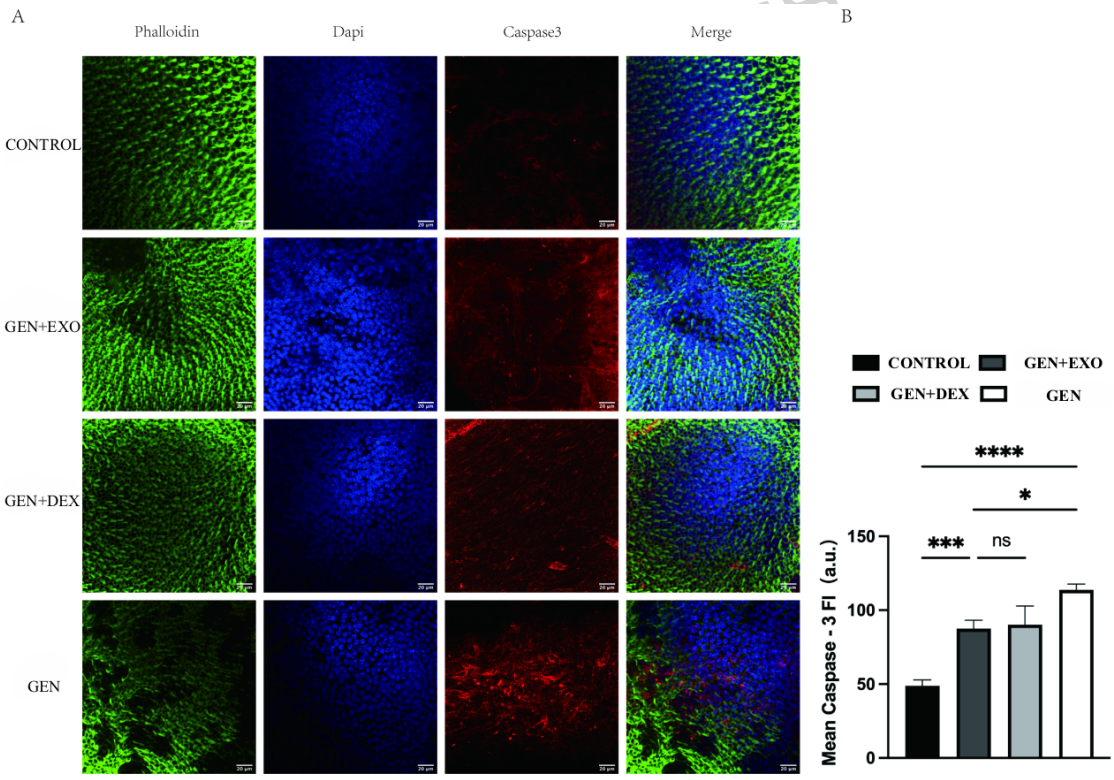

Figure 10 Caspase3 immunofluorescence staining images

A: Immunofluorescence staining images of Caspase3 in different groups. Phalloidin (green) labels actin, DAPI (blue) stains cell nuclei, and Caspase3 is stained red. The groups include Normal, GEN+EXO, GEN+DEX, and GEN; B: Statistical plot of fluorescence intensity analyzed by Image J software. *p < 0.05, **p < 0.01, ***p < 0.001, ****p < 0.0001; ns: no significant difference.

As shown in Figures 11A-B, the LC3 fluorescence signal intensity

in the control group remained at baseline levels, indicating that the autophagy-related protein LC3 is basally expressed under physiological conditions. After gentamicin intervention, LC3 fluorescence intensity significantly increased in the GEN+EXO, GEN+DEX, and GEN groups ($p<0.05$). The LC3 expression level in the GEN+EXO group showed a statistically significant difference compared to the GEN group ($p<0.01$), suggesting that exosome intervention enhances autophagic activity in hair cells within the gentamicin injury model.

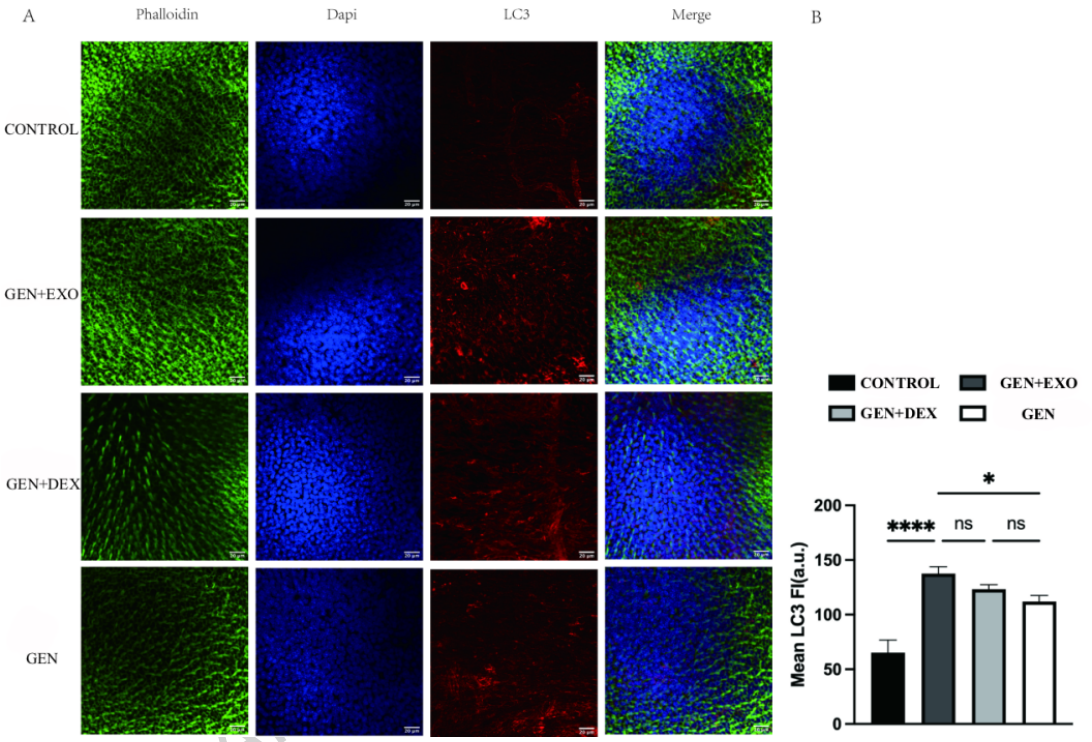

Figure 11 LC3 immunofluorescence staining images

A: Immunofluorescence staining images of LC3 in various groups. Phalloidin (green) labels actin, DAPI (blue) stains cell nuclei, and LC3 is visualized in red. The groups are Normal, GEN+EXO, GEN+DEX, and GEN; B: Statistical plot of fluorescence intensity analyzed by Image J software.*$p < 0.05$, **$p < 0.01$, ***$p < 0.001$, ****$p < 0.0001$; ns: no significant difference.

4. Discussion

This study focused on the clinical challenge posed by the non-regenerative nature of vestibular hair cells in mammals. Damage to these cells led to sequelae such as balance disorders and vertigo syndromes, and no effective interventions were available at the time of this research.[11]. The complex anatomy of vestibular organs and the presence of the blood-labyrinth barrier further hinder traditional drug therapy due to low delivery efficiency and poor targeting [12]. In recent years, mesenchymal stem cell-derived exosomes have

garnered significant attention for their unique biological properties: they carry multiple neurotrophic factors (e.g., BDNF, GDNF) and pro-survival miRNAs, while activating endogenous repair mechanisms through paracrine effects [13, 14]. Notably, most existing studies have validated the protective effects of stem cell exosomes on hair cell-like cells using in vitro culture systems, but key questions regarding in vivo trans-barrier delivery efficiency, tissue residence duration, and systemic regulatory mechanisms remain unclear.

A breakthrough of this study was the first demonstration in a live animal model that hucMSC-EXOs were delivered via intratympanic injection, which penetrates the round window membrane and oval window to directly enter vestibular end organs without crossing the blood-labyrinth barrier. This route enhances local exosome concentration (highest in the saccular macula) and reduces systemic metabolism-related drug loss, consistent with previous mechanisms of intratympanic administration for inner ear diseases,maintain bioactivity within vestibular organs, and exert sustained therapeutic effects. More importantly, through systematic behavioral assessments including the rotarod beam test and open-field test, we provided the first in vivo evidence that mesenchymal stem cell vesicles significantly suppressed gentamicin-induced vestibular dysfunction offering critical preclinical evidence for translational medicine research.

4.1 Intratympanic injection of hucMSC-Derived Exosomes Enables Targeted Delivery to Vestibular Sensory Epithelium

While previous studies have highlighted exosomes as superior nanocarriers due to low immunogenicity, minimal cumulative toxicity, strong barrier-crossing ability, high bioavailability, stability, and ease of storage [15], direct evidence for their efficacy in vestibular system research has been lacking. For example, exosome-encapsulated adeno-associated virus (exo-AAV) has shown enhanced transfection efficiency in inner hair cells [16], but this does not confirm direct delivery to the vestibular system.

This study for the first time demonstrated that exosomes administered via intratympanic injection could successfully reach the sensory epithelium of vestibular end organs and undergo cellular internalization. This not only validated the feasibility of exosomes as trans-barrier carriers for vestibular interventions but also established a foundation for exploring their role in treating vestibular disorders or modulating physiological functions. The discovery further suggested that exosomes might serve as ideal carriers for delivering therapeutic agents or regulatory factors to the vestibular system, offering advantages over viral vectors (e.g., AAV) in immunogenicity and artificial nanoparticles in potential toxicity, particularly for chronic

vestibular injuries requiring repeated administration

4.2 hucMSC-Derived Exosomes Suppress Gentamicin-Induced Vestibular Dysfunction

The open-field test comprehensively assessed autonomous activity and exploratory behavior. Control rats exhibited active movement with broad activity ranges and complex trajectories, whereas GEN rats showed significantly inhibited activity, as visually evident in heat maps and track plots. The GEN+EXO group demonstrated significant improvements in total movement distance and speed compared to the GEN group, but both GEN+EXO and GEN+DEX groups showed no recovery in center zone entry frequency, remaining significantly lower than the control group. This suggests that exploratory behavior, which involves complex neuroregulation and psychological factors (e.g., emotional state, environmental cognition, stress response) [17], may require deeper modulation than what exosomes or dexamethasone can achieve, indicating limitations in overcoming gentamicin-induced damage to related neural pathways or psychological states.

The beam balance test evaluated neurocoordination and balance ability, with three distinct movement patterns (smooth walking, hindlimb dragging, frequent falling) directly correlating with passage time. On day 3, no significant differences were observed among groups, likely due to early-stage compensation masking injury effects and insufficient treatment accumulation. By day 6, GEN rats exhibited a marked increase in passage time (23.83 seconds vs. 8.40 seconds in controls), confirming severe and persistent balance dysfunction. Both GEN+EXO and GEN+DEX groups showed significant reductions in passage time compared to GEN, with comparable efficacy between treatments. The control group’s shorter passage time on day 6 reflected motor skill improvement through training, whereas the GEN group’s prolonged time underscored the irreversible nature of gentamicin-induced vestibular damage, unaffected by compensatory mechanisms or training effects.

4.3 hucMSC-Derived Exosomes Alleviate Gentamicin-Induced Hearing Loss

Auditory brainstem response (ABR) testing revealed that the GEN+EXO group exhibited significantly lower ABR thresholds at 32 kHz compared to the GEN group, comparable to the GEN+DEX group, indicating both interventions effectively mitigate gentamicin-induced high-frequency hearing loss. This aligns with published mechanisms showing exosomes protect cochlear hair cells via anti-apoptosis, anti-oxidation, and autophagy promotion [10], with ABR threshold differences at 32 kHz consistent with prior reports [10]. No significant differences were observed at 4–24 kHz or with click stimuli, likely

because tympanic administration primarily targets the basal turn of the basilar membrane (corresponding to high-frequency hearing), whereas other frequency regions are less affected by local drug delivery.

4.4 hucMSC-Derived Exosomes Mitigate Gentamicin-Induced Vestibular Hair Cell Damage

Previous studies on hair cell counting in the utricle and saccule typically focused only on the striolar and extrastriolar regions [18, 19], as gentamicin-induced vestibular hair cell damage exhibits significant regional specificity, closely linked to the subtype distribution and characteristics of vestibular hair cells. In mammals, both type I and type II hair cell subtypes exist in the central and peripheral regions of vestibular end organs, with nearly equal proportions in peripheral regions, while type I hair cells are more abundant in the striolar region [20]. Type I hair cells are more susceptible to gentamicin damage [21]. However, preliminary exploration in this study revealed a significant decrease in hair cell density in the medial extrastriola of the utricle after gentamicin injury, differing from the lateral extrastriola. Based on this finding, independent counting of the medial and lateral extrastriola of the utricle was performed, clearly demonstrating significant post-injury differences in the medial extrastriola.

Scanning electron microscopy (SEM) further corroborated these results at the microstructural level. In the GEN group, SEM showed severe damage to hair cell surfaces, with extensive cilia loss and dense pitted vacuoles remaining on the cell surface, visually indicating severe disruption of cilia and surface structures.

The GEN+EXO group exhibited significant therapeutic effects in the striolar region (S) of the utricle, saccular striola, and crista ampullaris, with notable improvements in the medial extrastriola (MES) of the saccule. Although the average hair cell count in the utricular S and crista ampullaris S regions was lower in the GEN+EXO group than in the GEN+DEX group, the saccular striolar region showed higher counts in GEN+EXO. This may be related to the anatomical locations of vestibular end organs and drug distribution: intratympanic injection results in uneven drug distribution across maculae, following the pattern saccular macula > utricular macula > crista ampullaris [22]. Such distribution differences likely contribute to the varying therapeutic effects of exosomes across regions. The relatively higher accumulation of exosomes in the saccular macula provides a material basis for their stronger reparative effect on saccular striolar hair cells, while lower exosome distribution in the utricular MES and saccular extrastriola (ES) may lead to fewer hair cells compared to the GEN+DEX group due to less effective drug

delivery.

4.5 Proteomics Reveals Exosomes Improve Gentamicin-Induced Vestibular Injury via SNARE Pathway and Autophagy Activation

KEGG pathway analysis identified the complement and coagulation cascade as the most significantly altered pathway in the GEN group, indicating that gentamicin-induced inner ear injury involves cross-activation of the complement system and coagulation cascade. This finding aligns with QiLi et al.'s study [23], which enriched 1,083 target genes from idiopathic sudden deafness patients into metabolic and complement-coagulation cascade pathways, though the study did not further elaborate on the pathway-disease correlation. The complement-coagulation cascade represents molecular cross-talk between the immune and coagulation systems, both of which are plasma protease cascade systems forming an "inflammation-coagulation" vicious cycle through zymogen activation, cascade amplification, and shared regulatory factors [24]. Combined with the HIF-1 pathway enriched by network toxicology, the mechanism can be traced to a triple injury pathway: First, gentamicin directly damages stria vascularis endothelial cells, increasing blood-labyrinth barrier permeability, while activating the complement classical pathway via mitochondrial oxidative stress to release anaphylatoxins like C3a and C5a [25]. Second, C5a recruits neutrophils to the vestibular sensory epithelium, releasing reactive oxygen species (ROS) and activating the NLRP3 inflammasome, exacerbating hair cell apoptosis. Complement components also promote Th17 cell differentiation, whose secreted IL-17 further activates coagulation factor XII, forming a "complement-coagulation-inflammation" positive feedback loop [26]. Additionally, coagulation system activation forms microthrombi, synergizing with gentamicin-induced mitochondrial dysfunction to cause local inner ear hypoxia and activate the HIF-1 pathway. HIF-1α transcriptionally upregulates C3, C5a receptors, and tissue factor (TF), further reinforcing the complement-coagulation cascade [27] and establishing an "hypoxia-inflammation-coagulation" vicious cycle.

The GEN+EXO group showed significant enrichment in the SNARE interaction pathway in vesicular transport. Through fusion of surface SNARE proteins (e.g., Syntaxin-4) with hair cell membranes, exosomes enhance endocytic efficiency while regulating Atg8-PE lipidation to promote autophagosome maturation [28]. This mechanism specifically clears gentamicin-induced damaged mitochondria (mitophagy), reduces ROS production, and inhibits upstream signals of complement activation (e.g., mitochondrial DNA release) [29]. Concurrently, exosome-carried Annexin A1 inhibits C5

convertase activity to reduce C5a generation and blocks HIF-1α transcriptional activation of complement components by downregulating HIF-1α protein stability [30]. In contrast to GEN+DEX, where dexamethasone inhibits NF-κB-mediated inflammatory factor expression via glucocorticoid receptors [31], it fails to effectively regulate autophagic flux. Exosomes, however, achieve selective degradation of damaged components through autophagy, avoiding proteasome overload and explaining their superior safety and regional specificity in hair cell repair.

4.6 Exosomes Reduce Vestibular Hair Cell Apoptosis by Inhibiting Caspase-3 Expression and Enhance Autophagic Activity by Upregulating LC3 Signaling

LC3, as an autophagy marker protein, its expression level directly reflects cellular autophagic activity [32]; caspases, particularly Caspase-3, as key proteases in the execution phase of apoptosis, their activation and expression accurately indicate the apoptosis process [33]. Immunofluorescence detection of these two markers allows in-depth exploration at the cellular and molecular levels whether exosomes regulate autophagic and apoptotic abnormalities induced by gentamicin ototoxicity, thereby validating the potential mechanism of exosomes in ameliorating gentamicin ototoxicity through anti-apoptosis and autophagy enhancement.

In the control group, low Caspase-3 fluorescence intensity in vestibular hair cells indicated normal low-apoptosis levels [34]. The significantly enhanced Caspase-3 fluorescence in the GEN group clearly demonstrated that gentamicin induces vestibular hair cell apoptosis, consistent with previous studies on gentamicin ototoxicity mechanisms. Gentamicin may activate intracellular apoptotic signaling pathways through multiple mechanisms, such as damaging mitochondrial function, leading to cytochrome C release, activating the caspase cascade, and ultimately inducing apoptosis [35]. The significantly reduced Caspase-3 fluorescence intensity in the GEN+EXO group compared to the GEN group strongly confirms that exosomes effectively inhibit gentamicin-induced hair cell apoptosis. Exosomes are rich in bioactive molecules (e.g., proteins, nucleic acids, lipids), which may exert anti-apoptotic effects through multiple mechanisms [36]. For example, exosomes may deliver anti-apoptotic proteins or miRNAs into damaged cells, regulating intracellular apoptotic signaling pathways by inhibiting pro-apoptotic protein expression or activating anti-apoptotic protein functions to block apoptosis [37, 38]. The GEN+DEX group also showed lower Caspase-3 fluorescence than the GEN group but slightly higher than GEN+EXO. As a classic glucocorticoid, dexamethasone exhibits anti-inflammatory and anti-apoptotic effects by binding to intracellular

glucocorticoid receptors, regulating gene transcription, and inhibiting inflammatory factor release and apoptosis-related protein expression [39-41].

Autophagy is a critical self-protective mechanism that maintains cellular homeostasis by degrading and recycling damaged organelles and protein aggregates. In this study, the GEN+EXO group showed significantly higher LC3 fluorescence intensity than the GEN group, indicating exosomes promote autophagy. This aligns with prior reports that exosomes enhance autophagy via increased endocytosis [10, 42-44]. No significant difference was observed between the GEN+DEX and GEN groups, possibly due to dexamethasone's concentration-dependent effects on autophagy [45]. Notably, the GEN group exhibited elevated autophagic activity compared to the control group, likely representing a stress-induced compensatory response to toxicity. However, this compensatory autophagy was insufficient to counteract gentamicin-induced apoptotic cascades, ultimately leading to massive hair cell death.

5. Conclusions

Intratympanic injection of hucMSC-EXOs and dexamethasone both reached the utricular macula, saccular macula, and crista ampullaris, significantly improving gentamicin-induced balance dysfunction and alleviating high-frequency hearing loss. hucMSC-EXOs exhibited superior efficacy compared to dexamethasone in open-field test movement speed and hair cell count in the saccular striolar region.

Proteomics analysis revealed that the mechanism of gentamicin-induced inner ear injury may be associated with inflammatory damage triggered by the complement-coagulation cascade. Exosomes significantly improved gentamicin-induced vestibular dysfunction and hair cell injury by inhibiting Caspase-3-mediated apoptosis and activating the SNARE pathway to enhance autophagy.

6. Ethical Statement

6.1 Funding

This study was supported by the Beijing Natural Science Foundation (Grant No. 7222185), the Fund of Liaoning Provincial Education Department (Grant No. JYTMS20230575), the National Natural Science Foundation of China (Grant No. 82072953), the Top Young Talent Program of Liaoning Provincial Government (Grant No. XLYC1907009), and the Dalian Outstanding Young Talents Project (Grant No. 2021RJ12).

6.2 Ethical approval and consent to participate

The mesenchymal stem cell-derived exosomes used in this

study are sourced from a research project that has obtained ethical approval. The source project (title: Clinical Study on Umbilical Cord Mesenchymal Stem Cells in the Treatment of Acute Ischemic Stroke) was reviewed and approved by the Ethics Committee of the Stem Cell Clinical Research Institution, the First Affiliated Hospital of Dalian Medical University, with the approval number 2022-01 and the approval date of January 16, 2022. This study only involves the use of the aforementioned exosomes and does not involve human samples or human participation, thus there is no need to obtain written informed consent from patients or their guardians/legally authorized representatives.

6.3Animal Ethics Statement

The animal study was approved by the Medical Ethics Committee of PLA General Hospital, with the project title “Research on Intelligent Recognition of Auditory Brainstem Evoked Potentials Based on Deep Learning” and approval date on March 2, 2021. The approval number is S2020-465-01. All procedures were conducted in accordance with relevant guidelines and regulations.

6.4Clinical Trial Registration

Clinical trial number: not applicable.

6.5Acknowledgments

The proteomics experiments (including sample processing, mass spectrometry analysis, and bioinformatics analysis) were outsourced to Shanghai Baipu Biotechnology Co., Ltd., and animal samples were collected by the authors.The authors declare that they did not use AI-generated work in this manuscript.

7. References

[1] Rameshsankar S, Seethapathy J, Balakrishnan U. Ototoxic Drug Exposure and Hearing Loss in Neonates: A Scoping Review [J]. Am J Audiol, 2024, 33(4): 1356-77.

[2] Jiang X, Li W, Zang H, et al. [Apoptosis and its molecular mechanism in vestibular hair cell after gentamycin toxicity] [J]. Lin Chuang Er Bi Yan Hou Ke Za Zhi, 2005, 19(19): 886-9.

[3] Hu R, Wu F, Zheng Y Q. Ivacaftor attenuates gentamicin-induced ototoxicity through the CFTR-Nrf2-HO1/NQO1 pathway [J]. Redox Rep, 2024, 29(1): 2332038.

[4] Akila A A, Gad R A, Ewees M G E, et al. Clopidogrel protects against gentamicin-induced nephrotoxicity through targeting oxidative stress, apoptosis, and coagulation pathways [J]. Naunyn Schmiedebergs Arch Pharmacol, 2025, 398(3): 2609-25.

[5] Zheng H, Zhu R, Zhang Y, et al. Protective Effect of Marine Peptide from Netunea arthritica cumingii Against Gentamicin-Induced Hair

Cell Damage in Zebrafish [J]. Mar Drugs, 2024, 22(11).
[6] Watanuki K, Stupp H F, Meyer zum Gottesberge A. Toxic effects of gentamycin upon the peripheral vestibular sensory organs [J]. Laryngoscope, 1972, 82(3): 363-71.
[7] Ferreira K, Forbes S, Kaski D. Vestibulotoxicity with gentamicin [J]. Bmj, 2022, 378: e070873.
[8] Mei R, Wan Z, Yang C, et al. Advances and clinical challenges of mesenchymal stem cell therapy [J]. Front Immunol, 2024, 15: 1421854.
[9] Xia J, Minamino S, Kuwabara K, et al. Stem cell secretome as a new booster for regenerative medicine [J]. Biosci Trends, 2019, 13(4): 299-307.
[10] Liu H, Kuang H, Wang Y, et al. MSC-derived exosomes protect auditory hair cells from neomycin-induced damage via autophagy regulation [J]. Biol Res, 2024, 57(1): 3.
[11] Qi J, Huang W, Lu Y, et al. Stem Cell-Based Hair Cell Regeneration and Therapy in the Inner Ear [J]. Neurosci Bull, 2024, 40(1): 113-26.
[12] Koehler K R, Nie J, Longworth-Mills E, et al. Generation of inner ear organoids containing functional hair cells from human pluripotent stem cells [J]. Nat Biotechnol, 2017, 35(6): 583-9.
[13] Zhou Y, Seo J, Tu S, et al. Exosomes for hair growth and regeneration [J]. J Biosci Bioeng, 2024, 137(1): 1-8.
[14] Ha D H, Kim H K, Lee J, et al. Mesenchymal Stem/Stromal Cell-Derived Exosomes for Immunomodulatory Therapeutics and Skin Regeneration [J]. Cells, 2020, 9(5).
[15] Baruah H, Sarma A, Basak D, et al. Exosome: From biology to drug delivery [J]. Drug Deliv Transl Res, 2024, 14(6): 1480-516.
[16] György B, Sage C, Indzhykulian A A, et al. Rescue of Hearing by Gene Delivery to Inner-Ear Hair Cells Using Exosome-Associated AAV [J]. Mol Ther, 2017, 25(2): 379-91.
[17] Koçkaya M, Isparta S, Reinhardt P R, et al. Correction to: Tracking puppy development: automated analysis and qualitative behavioral assessment in repeated open field tests [J]. Vet Res Commun, 2024, 49(1): 47.
[18] Chiba M, Ito T, Shinkawa C, et al. Consistent removal of hair cells in vestibular end organs by time-dependent transtympanic administration of gentamicin in guinea pigs [J]. J Neurosci Methods, 2021, 351: 109049.
[19] Stewart C, Yu Y, Huang J, et al. Effects of high intensity noise on the vestibular system in rats [J]. Hear Res, 2016, 335: 118-27.
[20] Warchol M E, Massoodnia R, Pujol R, et al. Development of hair cell phenotype and calyx nerve terminals in the neonatal mouse utricle [J]. J Comp Neurol, 2019, 527(11): 1913-28.

[21] Lopez I, Honrubia V, Lee S C, et al. Quantification of the process of hair cell loss and recovery in the chinchilla crista ampullaris after gentamicin treatment [J]. Int J Dev Neurosci, 1997, 15(4-5): 447-61.
[22] Zhang R. Study on the Distribution and Damage of Gentamicin Injection in the Peripheral Vestibule via Tympanic Cavity [Master's thesis]. 2010.[23] Li Q, Peng X, Huang H, et al. RNA sequencing uncovers the key microRNAs potentially contributing to sudden sensorineural hearing loss [J]. Medicine (Baltimore), 2017, 96(47): e8837.
[24] Rawish E, Sauter M, Sauter R, et al. Complement, inflammation and thrombosis [J]. Br J Pharmacol, 2021, 178(14): 2892-904.
[25] Schäfer N, Grässel S. Involvement of complement peptides C3a and C5a in osteoarthritis pathology [J]. Peptides, 2022, 154: 170815.
[26] Luciano M, Sieberer H, Krenn P W, et al. Targeting NLRP3 inhibits AML progression by inducing PERK/eIF2-mediated apoptosis [J]. Cell Commun Signal, 2024, 22(1): 424.
[27] Fei J, Qin X, Ma H, et al. Resveratrol Ameliorates Deep Vein Thrombosis-Induced Inflammatory Response Through Inhibiting HIF-1α/NLRP3 Pathway [J]. Inflammation, 2022, 45(6): 2268-79.
[28] Li R, Pang L. An interplay between biomolecular condensates and SNARE proteins regulates plant autophagy [J]. Autophagy, 2024, 20(12): 2833-5.
[29] Kuznetsov A V, Margreiter R, Ausserlechner M J, et al. The Complex Interplay between Mitochondria, ROS and Entire Cellular Metabolism [J]. Antioxidants (Basel), 2022, 11(10).
[30] Zheng Y, Li Y, Li S, et al. Annexin A1 (Ac2-26)-dependent Fpr2 receptor alleviates sepsis-induced acute kidney injury by inhibiting inflammation and apoptosis in vivo and in vitro [J]. Inflamm Res, 2023, 72(2): 347-62.
[31] Wang Q, Xu B, Fan K, et al. Inflammation suppression by dexamethasone via inhibition of CD147-mediated NF-κB pathway in collagen-induced arthritis rats [J]. Mol Cell Biochem, 2020, 473(1-2): 63-76.
[32] Peña-Martinez C, Rickman A D, Heckmann B L. Beyond autophagy: LC3-associated phagocytosis and endocytosis [J]. Sci Adv, 2022, 8(43): eabn1702.
[33] Wu Y, Xv Y, Zhao L, et al. PSTK exerts protective role in cisplatin-tubular cell injury via BAX/BCL2/Caspase3 pathway [J]. Physiol Rep, 2025, 13(1): e70162.
[34] Muderris T, Yar Sağlam A S, Unsal D, et al. Efficiency of resveratrol in the prevention and treatment of age-related hearing loss [J]. Exp Ther Med, 2022, 23(1): 40.

[35] Steyger P S. Mechanisms of Ototoxicity and Otoprotection [J]. Otolaryngol Clin North Am, 2021, 54(6): 1101-15.
[36] Lai J J, Chau Z L, Chen S Y, et al. Exosome Processing and Characterization Approaches for Research and Technology Development [J]. Adv Sci (Weinh), 2022, 9(15): e2103222.
[37] Doyle L M, Wang M Z. Overview of Extracellular Vesicles, Their Origin, Composition, Purpose, and Methods for Exosome Isolation and Analysis [J]. Cells, 2019, 8(7).
[38] Zaborowski M P, Balaj L, Breakefield X O, et al. Extracellular Vesicles: Composition, Biological Relevance, and Methods of Study [J]. Bioscience, 2015, 65(8): 783-97.
[39] Takeda T, Takeda S, Kakigi A. Effects of Glucocorticoids on the Inner Ear [J]. Front Surg, 2020, 7: 596383.
[40] Gao Z, Schwieger J, Matin-Mann F, et al. Dexamethasone for Inner Ear Therapy: Biocompatibility and Bio-Efficacy of Different Dexamethasone Formulations In Vitro [J]. Biomolecules, 2021, 11(12).
[41] Nguyen T N, Yoo S Y, Tangchang W, et al. Sustained delivery of triamcinolone acetonide from a thermosensitive microemulsion gel system for the treatment of sensorineural hearing loss [J]. Drug Deliv, 2023, 30(1): 2242003.
[42] Skotland T, Sandvig K, Llorente A. Lipids in exosomes: Current knowledge and the way forward [J]. Prog Lipid Res, 2017, 66: 30-41.
[43] Cheng C, Wu Y, Huang Y, et al. Epigenetic modification and exosome effects on autophagy in osteoarthritis [J]. Biochem Pharmacol, 2023, 218: 115930.
[44] Buratta S, Tancini B, Sagini K, et al. Lysosomal Exocytosis, Exosome Release and Secretory Autophagy: The Autophagic- and Endo-Lysosomal Systems Go Extracellular [J]. Int J Mol Sci, 2020, 21(7).
[45] Martinelli S, Anderzhanova E A, Bajaj T, et al. Stress-primed secretory autophagy promotes extracellular BDNF maturation by enhancing MMP9 secretion [J]. Nat Commun, 2021, 12(1): 4643.